Detection of embedded ultra-subwavelength-thin dielectric features using elongated photonic nanojets

César Méndez Ruiz and Jamesina J. Simpson*

Department of Electrical and Computer Engineering, University of New Mexico, 1 University of New Mexico, Albuquerque, NM, 87131, USA
**simpson@ece.unm.edu*

Abstract: Photonic nanojets have been previously shown (both theoretically and experimentally) to be highly sensitive to the presence of an ultra-subwavelength nanoscale particle within the nanojet. In the present work, photonic nanojets elongated by almost an order of magnitude (relative to the latest previously published work) are found to possess another key characteristic: they are sensitive to the presence of ultra-subwavelength nanoscale thin features embedded within a dielectric object. This additional characteristic of photonic nanojets is demonstrated through comparisons between fundamentally different 3-D and corresponding 1-D full Maxwell's equations finite-difference time-domain (FDTD) models.

©2010 Optical Society of America

OCIS codes: (170.0170) Medical optics and biotechnology; (170.1530) Cell analysis.

References and links

1. Z. Chen, A. Taflove, and V. Backman, "Photonic nanojet enhancement of backscattering of light by nanoparticles: a potential novel visible-light ultramicroscopy technique," Opt. Express **12**(7), 1214–1220 (2004).
2. X. Li, Z. Chen, A. Taflove, and V. Backman, "Optical analysis of nanoparticles via enhanced backscattering facilitated by 3-D photonic nanojets," Opt. Express **13**(2), 526–533 (2005).
3. A. Heifetz, K. Huang, A. Sahakian, X. Li, A. Taflove, and V. Backman, "Experimental confirmation of backscattering enhancement induced by a photonic jet," Appl. Phys. Lett. **89**(22), 221118 (2006).
4. A. Heifetz, S.-C. Kong, A. V. Sahakian, A. Taflove, and V. Backman, "Photonic Nanojets," J Comput Theor Nanosci **6**(9), 1979–1992 (2009).
5. S.-C. Kong, A. Taflove, and V. Backman, "Quasi one-dimensional light beam generated by a graded-index microsphere," Opt. Express **17**(5), 3722–3731 (2009).
6. J. J. Simpson, "Extended Photonic Nanojets for Obtaining the Internal Composition of a Dielectric Slab," Proc. URSI National Radio Science Meeting, Boulder, CO, Jan. (2010).
7. J. J. Simpson, "Optical detection of a narrow ultra-subwavelength-thin dielectric layer via cepstral analysis of photonic nanojet backscattering," Proc. Photonics North, Niagara Falls, Canada, June (2010).
8. A. Taflove, and S. C. Hagness, *Computational Electrodynamics: The Finite-Difference Time Domain Method*, 3rd ed. (Norwood, MA: Artech House, 2005).
9. R. Nevels, and J. Jeong, "The time domain Green's function and propagator for Maxwell's equations," IEEE Trans. Antenn. Propag. **52**(11), 3012–3018 (2004).
10. J. F. Poco, and L. W. Hrubesh, "Method of producing optical quality glass having a selected refractive index," U.S. Patent 6,158,244, (2008).
11. Z. B. Wang, W. Guo, A. Pena, D. J. Whitehead, B. S. Luk'yanchuk, L. Li, Z. Liu, Y. Zhou, and M. H. Hong, "Laser micro/nano fabrication in glass with tunable-focus particle lens array," Opt. Express **16**(24), 19706–19711 (2008).
12. J. A. Roden, and S. D. Gedney, "Convolution PML (CPML): An efficieint FDTD implementation of the CFS-PML for arbitrary media," Microw. Opt. Technol. Lett. **27**(5), 334–339 (2000).

1. Introduction

A photonic nanojet [1–5] is a narrow, high-intensity beam of light that emerges from the shadow-side surface of a plane-wave-illuminated dielectric microsphere of diameter larger than the wavelength, λ. Photonic nanojets have previously been shown (both theoretically and experimentally) to exhibit a high degree of sensitivity to the presence of an ultra-subwavelength nanoscale particle. In the present work, photonic nanojets elongated by almost an order of magnitude (relative to the recent published work of [5]) are found to also be

#130170 - $15.00 USD Received 15 Jun 2010; revised 5 Jul 2010; accepted 13 Jul 2010; published 23 Jul 2010
(C) 2010 OSA

sensitive to the presence of ultra-subwavelength nanoscale thin features embedded within a dielectric object. This additional characteristic of photonic nanojets [6,7] is demonstrated through comparisons between fundamentally different 3-D photonic nanojet models and their corresponding 1-D plane-wave illumination models. The full Maxwell's equations finite-difference time-domain (FDTD) [8] method is employed in all of the simulations of this Letter.

Comparisons between the 3-D and corresponding 1-D scenarios are made for the following reason: in a true 1-D universe, there is no near-field or far-field because the spatial dependence in time-domain of the 1-D Green's function is entirely contained in time-retarded Dirac delta functions [9]. In such a universe, an illuminated subwavelength-thin dielectric film would locally generate a high-spatial-frequency electromagnetic field distribution which would propagate to the end of the universe with zero attenuation or spreading. Information regarding the existence and characteristics of such a film could, in principle, be obtained at any remote location.

A key finding in the work of this Letter is that the 3-D physically-realizable photonic nanojet provides a sufficiently 1-D illumination of the scattering object. As a result, the photonic nanojet permits localized detection of embedded ultra-subwavelength inhomogeneities.

The remainder of this Letter is organized as follows. First, the relevant key characteristics of the photonic nanojet will be reviewed. The elongated photonic nanojet will then be introduced, followed by the results of 3-D FDTD calculations of the backscattering of a visible-light nanojet from a micron-scale dielectric cube having a deeply embedded, weakly contrasting (Δn = 0.1), film-like inhomogeneity of nanometer-scale thickness. It will be shown that the FDTD-computed backscattered cepstrum (the DFT of the spectrum, i.e. double DFT) of the nanojet clearly reveals the presence of such an ultra-sub-wavelength nano-thickness film. Furthermore, this cepstrum agrees very well with the FDTD-computed backscattered cepstrum of the corresponding (but physically, vastly different) 1-D plane-wave-illuminated, layered system. Hence, the photonic nanojet is shown to provide the desired nearly 1-D illumination.

Note that in this study, the backscattered cepstrum result is chosen over the spectrum curve because the object's characteristics may be more clearly extracted from the cepstrum curve than by examining the periodic backscattered spectrum.

2. The photonic nanojet

The narrow, high-intensity photonic nanojet that emerges from the shadow-side surface of a plane-wave-illuminated dielectric microsphere has been found to exhibit the following key properties [4,5]:

- Nanojet is capable of maintaining a subwavelength full-width at half-maximum (FWHM) at distances from the shadow-side surface of the dielectric microsphere that can extend more than ~2λ.
- Transverse beamwidth can be less than the classical diffraction limit, as small as ~λ/3.
- Inserting within a nanojet a nanoparticle of diameter d_n perturbs the far-field backscattered power of the illuminated microsphere by an amount that varies as d_n^3 for a fixed λ. This perturbation is much slower than the d_n^6 dependence of Rayleigh scattering for the same nanoparticle, if isolated and plane-wave illuminated.
- The d_n^3 perturbation behavior leads to the possibility of detecting a nanoparticle via its perturbation of the backscattering of the microsphere. The same nanoparticle would generally be undetectable if isolated and plane-wave illuminated at the same λ.

Figure 1, taken from Ref [4], vividly illustrates the final property above: extreme sensitivity of the amplitude of the backscattered nanojet to a nanoparticle perturbation. In this example, a 3.5 μm-diameter dielectric sphere of refractive index n = 1.59 is illuminated in an

#130170 - $15.00 USD Received 15 Jun 2010; revised 5 Jul 2010; accepted 13 Jul 2010; published 23 Jul 2010
(C) 2010 OSA

infinite vacuum region by an *x*-polarized, *z*-propagating plane wave of λ = 400 nm. A d_n = 20 nm gold nanoparticle moving along the dotted path causes a peak backscattered power perturbation of + 40% relative to the backscattered power of the isolated microsphere. This perturbation is only 4 dB below the full backscattered power of the isolated microsphere, and is caused by a nanoparticle that is 175-times smaller than the microsphere in diameter, and hence more than 30,000-times smaller than the microsphere in cross-section area. In effect, *the nanojet projects the presence of the nanoparticle to the far field.*

Later, Sections 4 and 5 will demonstrate that the backscattered cepstrum of the photonic nanojet is similarly sensitive to the presence of embedded nanoscale-thickness dielectric inhomogeneities within the nanojet.

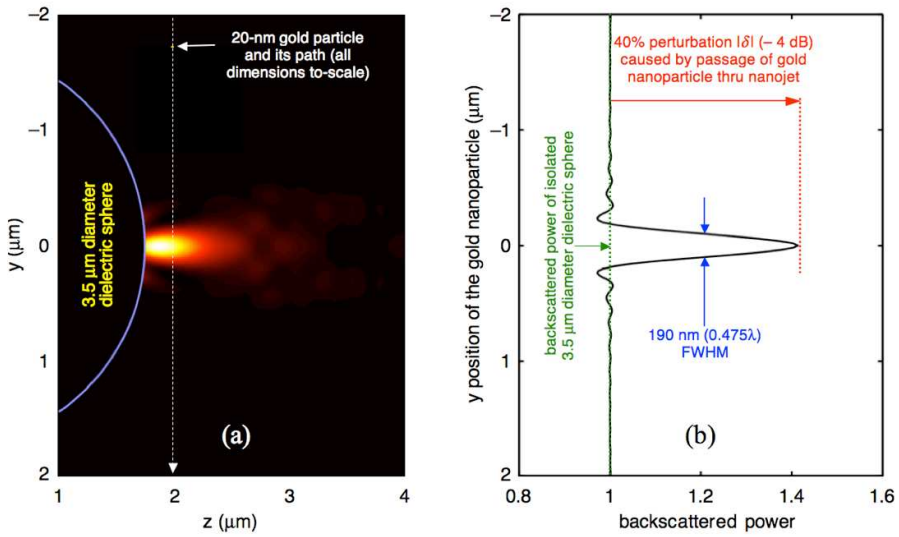

Fig. 1. Extreme sensitivity of the amplitude of a backscattered nanojet to a gold nanoparticle. The dotted path is 240 nm from the microsphere surface at the closest point [4].

3. The elongated photonic nanojet

Reference [5] showed how the length of the photonic nanojet can be increased to several microns by radially grading the refractive index of the generating microsphere. In conducting the 3-D FDTD modeling studies used in this paper, it was found that an even longer nanojet could be produced, up to ~20 μm, using an alternative radial grading. Figure 2 illustrates the results of such a grading for an x-polarized plane-wave-illuminated (λ = 500 nm) 5 μm diameter microsphere in free space, wherein six equally thick spherical shells are assumed. In order, from the outer shell to the inner core, the refractive indices here are *n* = 1.02, 1.04, 1.06, 1.08, 1.10, and 1.12. (These values of *n* are physically realizable using recent technology [10].) We note that the lengthening of the nanojet of Fig. 2 relative to the nanojet of Fig. 1 is at the expense of its widening in the transverse direction to a FWHM of 1.28 μm (~2.5λ). This is wider than the original nanojet's transverse width of ~λ/3, however utilizing the elongated nanojet, inhomogeneities located deeper inside the scattering object may be detected.

#130170 - $15.00 USD Received 15 Jun 2010; revised 5 Jul 2010; accepted 13 Jul 2010; published 23 Jul 2010
(C) 2010 OSA

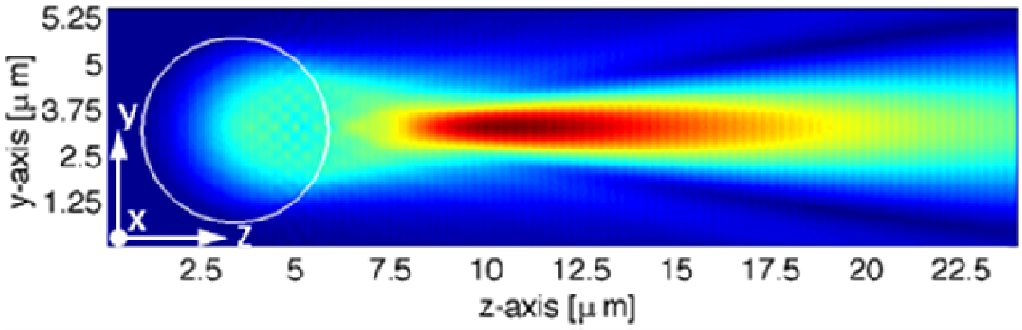

Fig. 2. Visualization of an elongated photonic nanojet generated by a plane-wave-illuminated, six-layer radially graded dielectric microsphere of 5 μm diameter. The incident wave is polarized along x-axis and propagates along the z-axis.

The difference between the radial grading used in this work and that of [5] is the contrast of the refractive index between each layer of the microsphere, and the lower average value of the microsphere layers. A second approach to changing the length of the nanojet is to alter the background medium as done in Wang et al. [11]. In this case, a homogeneous microsphere (n = 1.45332) surrounded by water (n = 1.326) yields a longer nanojet compared to when air is employed as the background media. That is, when the microsphere refractive index is closer in value to that of the background medium, the photonic nanojet is longer.

4. FDTD models

Figure 3 illustrates the geometry of the pure scattered-field 3-D FDTD model of the photonic nanojet of Fig. 2 interacting with a 2-μm dielectric cube of refractive index n = 1.3 centered upon the nanojet. The cube is assumed to be either homogeneous or have embedded at its midpoint a 25-nm-thin (λ/20) film-like inhomogeneity of index n = 1.4. The grid resolution is 25 nm, and a convolutional perfectly matched layer absorbing boundary condition eliminated numerical wave reflections from the outer grid boundary [12]. For each simulation case, the backscattered time-waveform is recorded 1.25 μm on the incident side of the microsphere for subsequent cepstral post-processing.

To permit a comparison between the 3-D case (Fig. 3) and a 1-D case, a pure scattered-field 1-D FDTD model having 25 nm grid resolution is constructed for a 2-μm-thick dielectric slab of refractive index n = 1.3 illuminated by a plane wave at normal incidence. The dielectric slab is similarly assumed to be either homogeneous or have a 25-nm-thin film-like inhomogeneity of refractive index n = 1.4 embedded at its midpoint. Finally, the reflected field time-waveform is similarly recorded 1.25 μm on the incident side of the dielectric slab for subsequent cepstral post-processing. The geometry for the corresponding 1-D scenario is illustrated in Fig. 4.

It is important to note that the 3-D and 1-D FDTD models studied herein have *fundamentally* different levels of complexity. For the 1-D model, the dielectric slab is normally and directly illuminated by a simple plane wave arriving from an infinite free-space region. Both the slab and the impinging wave extends infinitely without change in the transverse directions. On the other hand, for the 3-D model, a graded dielectric microsphere is interposed between the illuminating plane wave and the dielectric cube target. Electromagnetic wave propagation is computed in all possible directions within and around the dielectric microsphere, and within and around the dielectric cube. *Any* level of agreement between the results of these two widely disparate models would support the 1-D interaction hypothesis.

#130170 - $15.00 USD Received 15 Jun 2010; revised 5 Jul 2010; accepted 13 Jul 2010; published 23 Jul 2010
(C) 2010 OSA

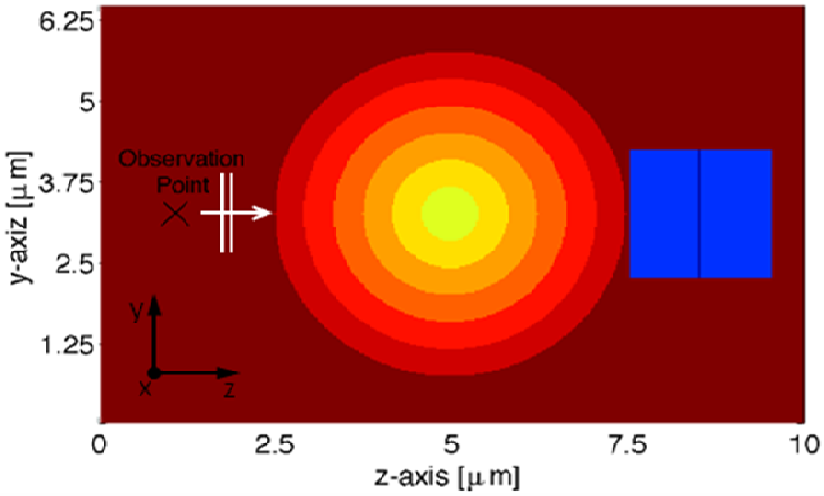

Fig. 3. 2-D slice of the geometry of a 3-D six-layer radially graded dielectric microsphere exciting the 2-μm test dielectric cube, here shown with the 25-nm-thin film-like inhomogeneity embedded at the middle of the z direction.

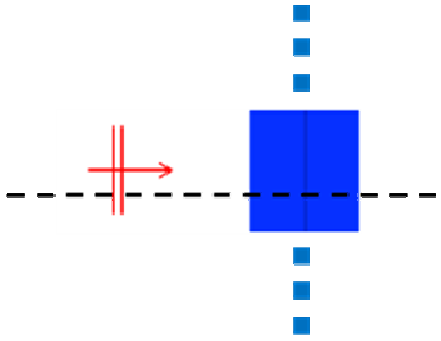

Fig. 4. 2-D example illustration of a slab having a dielectric thin film at its center analogous to the cube of Fig. 3. The dashed line represents the 1-D FDTD grid. The slab is illuminated via a plane wave, and the slab is infinite in the transverse directions to the incident plane wave.

5. Results

The first study involves a comparison of the backscattered response of the 3-D nanojet-illuminated n = 1.3 homogeneous cube and the 1-D plane-wave-illuminated n = 1.3 homogeneous slab. In the first step of the post-processing, a discrete Fourier transform (DFT) is applied to the backscattered field time-waveform of each geometry to generate the backscattered spectra. This step is followed by a second DFT operating upon the backscattered spectra, which yielded the backscattered cepstra.

Figure 5 compares the cepstra obtained in this manner for the 3-D nanojet-illuminated n = 1.3 homogeneous cube and the 1-D plane-wave-illuminated n = 1.3 homogeneous slab. A strong correlation between the two sets of results is observed. This is our first indication that the photonic nanojet is indeed providing a nearly one-dimensional interaction with the 3-D dielectric cube.

Cepstra resulting from the case wherein there is a 25 nm thin film-like inhomogeneity at the center of the n = 1.3 cube is shown in Fig. 6. Data corresponding to the 1-D model of the homogeneous cube was also included to emphasize the effect of the inhomogeneity. Again, there is a strong correlation between the results obtained from the 1-D and 3-D models.

#130170 - $15.00 USD Received 15 Jun 2010; revised 5 Jul 2010; accepted 13 Jul 2010; published 23 Jul 2010
(C) 2010 OSA

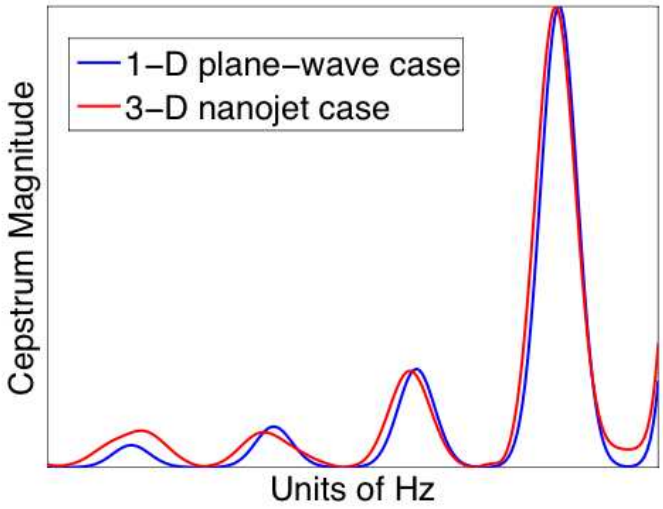

Fig. 5. Comparison of the cepstra of the 3-D nanojet-illuminated n = 1.3 homogeneous cube and the 1-D plane-wave-illuminated n = 1.3 homogeneous slab.

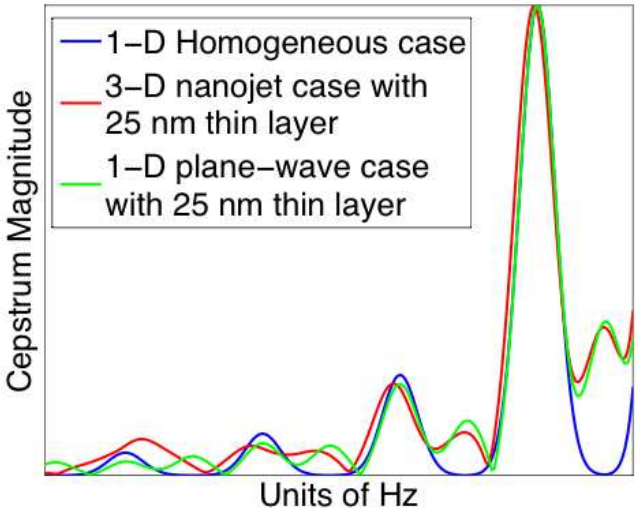

Fig. 6. Comparison of the cepstra as in Fig. 5, but now both the 3-D nanojet-illuminated cube and the 1-D plane-wave-illuminated slab have a 25-nm ($\lambda/20$) n = 1.4 film-like inhomogeneity embedded at their midpoint depths. For convenience, the nanojet-illuminated homogeneous cepstrum is also shown.

Comparing the results of Fig. 6 with the results of Fig. 5, we see that embedding the 25-nm n = 1.4 film at a midpoint depth within the cube and the slab causes a second set of cepstral peaks to arise. These new peaks occur primarily between the original cepstral peaks, and are of significant amplitude. Furthermore, there is an excellent agreement of the new peaks of the 3-D nanojet-illuminated cube and 1-D plane-wave-illuminated slab at the highest cepstral frequency. While this agreement diminishes with decreasing cepstral frequency, it remains significant down to the third new peak.

#130170 - $15.00 USD Received 15 Jun 2010; revised 5 Jul 2010; accepted 13 Jul 2010; published 23 Jul 2010
(C) 2010 OSA

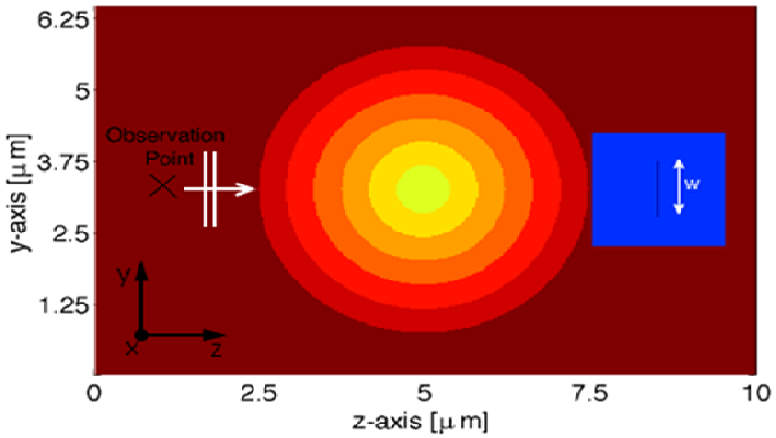

Fig. 7. Simulation geometry similar to that of Fig. 3 except that the transverse width (W) of the 25-nm-thin film-like inhomogeneity is varied.

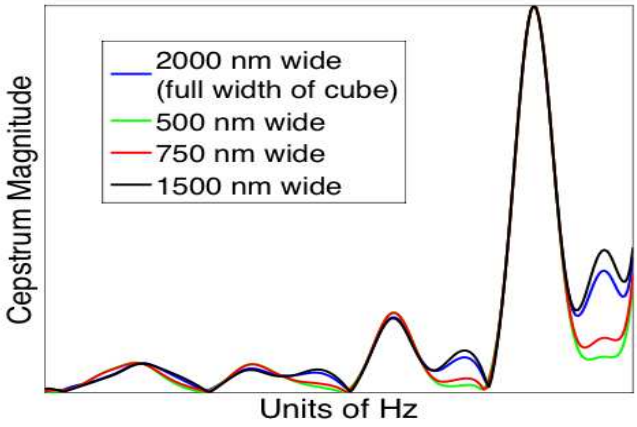

Fig. 8. Comparison of the 3-D nanojet cepstra according to the geometry of Fig. 7 for transverse widths of the 25-nm thin inhomogeneity at 500, 750, 1500 and 2000 nm.

Finally, Figs. 7 and 8 illustrate the geometry and cesptral results for a 25-nm thin film embedded at the dielectric cube's midpoint and having a transverse width of 500, 750, 1500, or 2000 nm. As expected, for transversely very narrow thin films, the second set of cepstral peaks corresponding to the thin layer diminish in amplitude, converging to the homogeneous dielectric cube result. Also, importantly, when the width of the film is varied, the location of the peaks does not shift in frequency. However, note in particular in Fig. 8 that the 1500 nm-wide film yields an increase in the second set of peaks with respect to those obtained with the 2000 nm wide film. This amplitude increase for the 1500-nm case is found to result from the interaction of the nanojet with the combination of the edges of the thin film and the longitudinal faces of the n = 1.3 dielectric slab. That is shown in Fig. 9, wherein we see that side lobes are generated due to the relatively short transversal width of the dielectric cube relative to the FWHM of the photonic nanojet. In fact, when the 2 μm dielectric cube is widened to 10 μm (maintaining a longitudinal dimension of 2 μm), the side lobes are no longer generated. As a result, we also find that for this 10-μm wide case, the amplitude of the second set of cepstral peaks corresponding to the thin film inhomogeneity progressively

#130170 - $15.00 USD Received 15 Jun 2010; revised 5 Jul 2010; accepted 13 Jul 2010; published 23 Jul 2010
(C) 2010 OSA

diminish in amplitude as the thin film is progressively narrowed in the transverse direction (instead of seeing a rise for the 1500 nm-wide case).

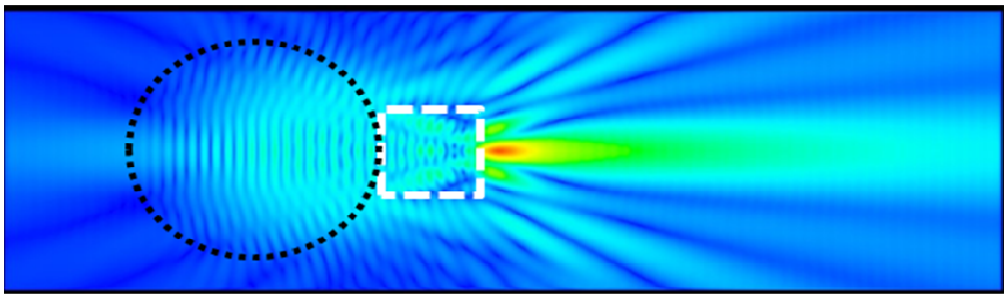

Fig. 9. Visualization of the dielectric sphere generating a photonic nanojet as shown in Fig. 2, but with a 2 μm dielectric cube located in the path of the nanojet. The incident wave is polarized along the x-axis and propagates along the z-axis, using the same coordinate system as defined in Fig. 7.

Note that these results were obtained using the elongated nanojet, which detects inhomogeneities at greater longitudinal distances at the expense of illuminating a wider transverse area of the object. Given the above observed interaction of the photonic nanojet with the edges of the thin film and longitudinal sides of the n = 1.3 dielectric cube, it may be advantageous to choose a narrower photonic nanojet to probe objects of relatively small transverse and longitudinal dimensions. The traditional (non-elongated) photonic nanojet has a transverse beamwidth at less than the classical diffraction limit, as small as ~λ/3. Thus, it may be used to probe shallower but also narrower transverse regions.

These results offer good evidence that the elongated photonic nanojet used in these studies indeed provides the action of a nearly one-dimensional beam over a significant range of cepstral frequencies. The nanojet allows the high spatial frequencies inherent in the fluctuations of the inhomogeneous near-field to be projected to the far-field in three dimensions in a manner consistent with its projection of a perturbing nanoparticle to the far-field (viz. Figure 1). And a backscattering scheme which emphasizes such a one-dimensional action does indeed provide means to detect ultra-subwavelength thin, weakly contrasting dielectric features deeply embedded within a surrounding material medium.

6. Conclusion and future work

In summary, this Letter demonstrated that the elongated photonic nanojet permits detection of an ultra-subwavelength-thin, weakly contrasting film-like inhomogeneity embedded in a 3-D material object via 1-D illumination and detection. As a possible consequence, the further development and application of photonic nanojets could provide useful new approaches for conducting inverse-scattering studies of weakly contrasting micron-scale material objects.

Future work will involve FDTD computational modeling of the interaction of photonic nanojets with multi-layer films and post-processing the backscattered field data to extract the dielectric layering properties, ordering, and thicknesses. Subsequent work will advance to transversely inhomogeneous, multi-layered films and analysis of the internal features of such films along different surface points. The ultimate phase will test the ability of photonic nanojets to detect nanometer-scale features within curved inhomogeneous dielectric objects.

Acknowledgement

Supercomputing resources were provided by the New Mexico Computing Applications Center and by the University of New Mexico's Center for Advanced Research Computing (CARC).

#130170 - $15.00 USD Received 15 Jun 2010; revised 5 Jul 2010; accepted 13 Jul 2010; published 23 Jul 2010
(C) 2010 OSA